Operating Region Extension of a Modular Multilevel Converter using Model Predictive Control: a Single Phase Analysis

Joan-Marc Rodriguez-Bernuz, *Student Member, IEEE,* Adrià Junyent-Ferré, *Member, IEEE,*

***Abstract*—The Modular Multilevel Converter (MMC) is the state-of-the-art topology for Voltage Source Converter HVDC (VSC-HVDC). Despite its advantages, this converter handles large internal low-frequency energy ripples and the capacitance that supports these dynamics is a key design parameter that affects the operating region of the converter. Different strategies can be found in literature to increase the feasible region of operation of the converter. Nevertheless, they are typically open-loop in nature and use pre-calculated control references. This paper presents an alternative based on Model Predictive Control (MPC) that steers the system through optimal control trajectories that are calculated online. This provides feedback and corrective control action in real time. The predictive controller used for this purpose is presented and a Linear Time-Varying (LTV) approximation is used to reduce the computational burden of the algorithm. The feasible boundaries of the converter are sought and the final performance of the control algorithm is evaluated through detailed simulations using a switching model of the converter.**

***Index Terms*—Modular Multilevel Converter (MMC), Model Predictive Control (MPC), Performance Optimization.**

NOMENCLAUTRE

Time-domain variables

$i_{(u,l)}$	Current through the upper and lower arms.
$i_{c(u,l)}$	Current through the equivalent arm capacitor.
i_{circ}	Circulating current.
i_g	AC grid current.
$v_{(u,l)}$	Voltage modulated at each arm.
$v_{(u,l)_{DC}}$	Voltage at each pole of the DC bus.
$v_{c(u,l)}$	Voltage of the equivalent arm capacitor.
v_g	AC grid voltage.
$e_{(u,l)}$	Instantaneous energy at each converter arm.
t	Time.
ω	Fundamental angular frequency.

Phasor-domain quantities

$I_{(u,l)}$	DC current component through upper and lower arms.
$\overline{I}_{(u,l)}$	Complex representation of the current in the upper and lower arms.
$\overline{I}_g$	Complex representation of the AC grid current.
$V_{(u,l)}$	DC voltage component in the upper and lower arms.
$V_{(u,l)_{DC}}$	DC component at each pole of the DC bus.
$\overline{V}_{(u,l)}$	Complex representation of the voltage modulated in the upper and lower arms.
$\overline{V}_g$	Complex representation of the AC grid voltage.
$\overline{Z}$	Complex representation of the grid impedance.
$\overline{Z}_a$	Complex representation of the arm impedance.

Converter parameters

E_N	Nominal arm energy.
I_p	Peak arm current.
C_a	Equivalent arm capacitance.
C_{SM}	Individual submodule capacitance.
N_{arm}	Number of submodules per arm.
L	AC grid filter resistance.
L_a	Arm inductance (upper or lower arm).
R	AC grid filter resistance.
R_a	Arm resistance (upper or lower arm).
SM	Submodule.
S_N	Nominal power
V_g	Nominal AC grid voltage.
V_{g_p}	AC grid peak voltage.
V_{DC}	Nominal DC bus voltage.
V_{SM}	Submodule nominal voltage.
V_{SM_p}	Submodule peak voltage.

Tuning parameters

Δt	Discrete sampling interval.
N	Length of the prediction horizon.
$\psi_{1,2,3}$	Scaling factors.
$\mathcal{R}, \mathcal{S}, \mathcal{U}$	Tuning weights.
λ_i	Softening variable.
λ_v	Softening variable.
λ_{v_c}	Softening variable.
$\mathcal{V}$	Safety margin on the modulated voltage.

Subscripts

h	Designates either the upper or lower arm.
k	Discrete time index.
l	Lower arm quantity.
u	Upper arm quantity.

Superscripts

$\sim$	Steady-state time-varying trajectory.
$*$	Designates reference variables.
$\wedge, \vee$	Hard constraints bounds.

Prefix

δ	Designates small-signal variables.

Joan-Marc Rodriguez-Bernuz and Adria Junyent-Ferré are with the Department of Electrical and Electronic Engineering, South Kensington Campus, Imperial College London, London SW7 2AZ, United Kingdom (e-mails: {j.rodriguez15, adria.junyent-ferre}@imperial.ac.uk)

I. Introduction

THE Modular Multilevel Converter (MMC) has become the converter topology adopted in many high-power applications, specially in High Voltage Direct Current (HVDC) transmission [1], [2]. The MMC is an interesting structure because of its scalability, which allows increasing the number of voltage levels by simply adding a larger number of submodules (SM) to each arm (see terminology in Fig. 1) [3], [4]. This reduces the filtering requirements, produces a clean output voltage and allows decreasing the switching frequency of the individual semiconductor devices which reduces their losses [1], [5]. In addition, the reliability of the system is enhanced as a large number of SMs would allow the converter to keep operating even in the event of a SM failure [3], [6]. The arm currents charge and discharge SM capacitors which results in periodic fluctuations in the energy stored in each arm. These energy oscillations contain different frequency components which generates non-negligible voltage ripple in the SMs capacitor. In order to guarantee a correct operation, the converter is designed to have a large SM capacitance such that the voltage ripple can be decreased. Nevertheless, the increment of the capacitance of the device has a direct impact on its size and cost, specially in high power applications [7]. While early work focused on the suppression of the circulating current within the converter [8], techniques based on controlled circulating current injection have been shown to reduce the voltage ripple of the SMs such that the energy storage requirements can be reduced [9]–[11]. Indeed, the increment of circulating current can be used to shape the energy oscillations without affecting the power exchanged with the AC system as long as the device efficiency is not compromised. Alternatively, the use of circulating current is also proposed to shape the arm capacitor ripple and extend the P-Q capability of the converter [12], [13]. This strategy has also been adopted in [14] to extend the dynamic overload capability of MMCs in HVDC systems. However, only the circulating current is considered in these analysis whilst other variables that could potentially enhance the device performance are not evaluated. In [15], all the different system variables that can increase the operating region of the MMC, i.e. circulating current, average energy stored and triplen harmonic injection in the case of three-phase systems, are discussed. This study proposed a control scheme which adapted a conventional open-loop controller while considering an appropriate set of internal variables as references. The steady-state values used as references were obtained from a numerical optimization algorithm based on a frequency-domain model of the MMC [16].

Alternatively, different publications propose the use of MPC techniques to control the MMC and regulate its circulating current [17], [18]. The implementation of MPC techniques in MMCs has gained attention in the last years due to its interesting features such as fast dynamics response and easiness to handle multivariable problems [19], [20]. Different MPC approaches based on Finite Control Set (FCS) strategies have been proposed, e.g. [21], [22], although existing FCS-MPC algorithms generally suffer from high computational burden when a large number of SMs is considered [23]. Nevertheless, recent publications suggest simplified strategies and/or the use of a modulator to extend the prediction horizon and reduce the burden of the optimization [24]. For instance, [25] introduces a novel approach where an MPC strategy is combined with a modulator achieving a regular pulse patter and improved steady-state tracking performance. Similarly, [26] presents an MPC current controller combined with a phase-shifted pulse-width modulation which decouples the burden of the predictive algorithm from the number of SMs. Similarly, this paper implements a predictive strategy combined with a modulator whose objective is to extend the operating region of an MMC. To do so, a long predictive horizon is stated to foresee whether or not the system states will reach physical constraints when the converter operates beyond its nominal design ratings. Besides, a Linear Time-Varying (LTV) strategy is proposed in order to reduce the burden of the optimization while retaining the main dynamics of the system [27].

This paper is organized as follows: Section II describes the system under analysis and provides insight into the modeling approach. Section III derives the time domain steady-state expressions required to formulate the predictive controller afterwards. Then, Section IV describes the MPC algorithm and formulates the LTV approximation. Section V compares the feasible operating region of the MMC when a conventional controller or the LTV-MPC approach are considered. Finally, the performance of the algorithm is evaluated in Section VI and some concluding remarks are given in Section VII.

II. General System Description and Modelling

The system under study, shown in Fig 1, is a single-phase MMC interfacing a DC link with an AC grid. A single-phase MMC is used in the analysis given that its dynamics are comparable to a three-phase MMC under balanced conditions. This statement is based on the analysis of the different currents through each arm of the MMC. This simplification does not detract the outcomes of the paper but facilitates the presentation of the predictive strategy as the complexity of the formulation and description of the algorithm is reduced.

Conventionally, each phase of the MMC is called leg, which is also subdivided into two subsystems called arms. Note that the upper and lower arms are designated with the sub-index u or l respectively. Each arm is comprised of a stack of N_{arm} series-connected SMs where each SM is a half-bridge converter although other topologies, such as the full-bridge, could be considered [4], [28]. The arms of the MMC are connected in series to an inductor, which smooths the arms current and limits its rate-of-change in case of faults. In addition, the middle point of the DC bus is connected to the neutral point of the AC side, providing a return path for the AC grid current.

The output voltage of the MMC is synthesized by setting the switching states of the SMs. If the number of SMs per arm is large, the harmonic content of the output voltage decreases and the high frequency distortion of the current can be attenuated easily [29]. The MMC has a large number of controllable degrees of freedom with as many independent voltages and

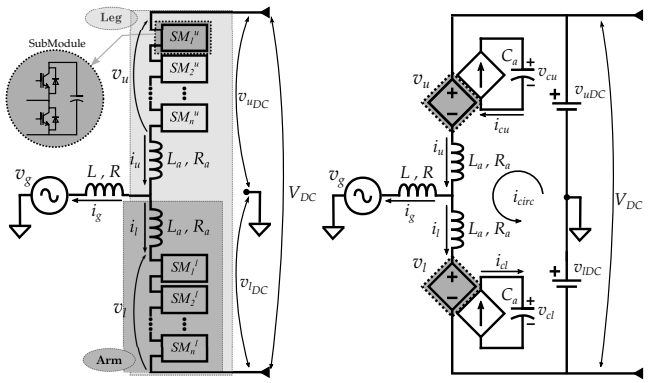

(a) Detailed schematic. (b) Average equivalent schematic.

Fig. 1. Illustrative schematics of a single-phase MMC.

switching signals as SMs in the converter. This fact increases the complexity of the modelling and the control design [30]. Commonly, the design of the controller relies on decoupling the system into different control problems. For instance, the time scales at which the current dynamics change are much smaller than those of the capacitor voltages. Therefore, the stack of SMs of each arm is typically regarded as a controllable voltage source in the design of the current controllers. Then, an energy controller acting significantly slower than the current controller is used to regulate the total energy of each arm [31]. To do so, the total capacitance of the arm is usually represented by an equivalent capacitor designated hereinafter as arm equivalent capacitor. This assumption is valid if all the capacitors of the arm are balanced [29]. The balancing of the stack of SMs is ensured by a slower-acting Balancing Control Algorithm (BCA) which equalizes the energy deviation of the SMs [32]. These simplifications lead to the equivalent schematic shown in Fig. 1b.

III. Steady-State Analysis of MMC

The steady-state analysis of the MMC is largely discussed in [29]. This analysis is used afterwards to determine the steady-state trajectories of the system in order to formulate the MPC algorithm introduced in Section IV. The following simplifications are considered:

- The AC grid is an ideal sinusoidal voltage source.
- The DC side is modeled as two constant voltage sources. The middle point of the DC link is grounded.
- The voltage modulated at each arm of the converter is not affected by the switching operation of the SMs.
- The losses of the converter are negligible.
- The SMs of each arm are correctly balanced.

A. Steady-State Equations

The analysis of the upper and lower meshes of the system depicted in Fig. 1b leads to the following expressions:

$$v_{u_{DC}} - v_u - v_g = +R_a\, i_u + L_a \frac{d}{dt} i_u + R\, i_g + L \frac{d}{dt} i_g \tag{1}$$

$$-v_{l_{DC}} + v_l - v_g = -R_a\, i_l - L_a \frac{d}{dt} i_l + R\, i_g + L \frac{d}{dt} i_g \tag{2}$$

where L_a and R_a are the arm inductance and its equivalent parasitic resistance. The sub-index *h = (u,l)* is used to designate those variables that correspond to the upper (*u*) or lower *(l)* arms respectively. Then, $v_{(h)_{DC}}$ is the the voltage of each pole of the DC bus, $v_{(h)}$ is the voltage modulated at each arm, $i_{(h)}$ is the current through each arm, i_g is the AC grid current and v_g is the AC grid voltage.

The dynamics of the equivalent arm capacitor are:

$$\frac{d}{dt} v_{c(h)} = \frac{i_{c(h)}}{C_a} = \frac{i_{(h)}\, v_{(h)}}{v_{c(h)}\, C_a} \tag{3}$$

where C_a is the arm equivalent capacitance, $v_{c(h)}$ is the voltage of the equivalent arm capacitor and $i_{c(h)}$ is the current through it. Note that the power balance within each arm ($i_{(h)}\, v_{(h)} = v_{c(h)}\, i_{c(h)}$) leads to (3).

Then, the grid current i_g is the difference of the arms current whilst the circulating current i_{circ} corresponds to the current common to both arms.

$$i_g = i_u - i_l \tag{4}$$

$$i_{circ} = \frac{i_u + i_l}{2} \tag{5}$$

1) AC component: as the voltage-current circuit relationships are linear, the analysis of the DC and AC system components can be performed independently. Then, the AC quantities are analyzed in the phasor-domain, decomposing them into real and imaginary parts.

The system impedances are defined as following:

$$\overline{Z} = R + j\omega L \tag{6}$$

$$\overline{Z}_a = R_a + j\omega L_a \tag{7}$$

where $\overline{Z}$ is the equivalent grid impedance, $\overline{Z}_a$ is the equivalent arm impedance and ω is the angular frequency of the grid.

Next, (1), (2), (4) and (5) are analysed in phasor-domain form:

$$-\Re\{\overline{V}_u\} = \Re\{\overline{V}_g - \overline{I}_u\, \overline{Z}_a - \overline{I}_g\, \overline{Z}\} \tag{8}$$

$$-\Im\{\overline{V}_u\} = \Im\{\overline{V}_g - \overline{I}_u\, \overline{Z}_a - \overline{I}_g\, \overline{Z}\} \tag{9}$$

$$\Re\{\overline{V}_l\} = \Re\{\overline{V}_g + \overline{I}_l\, \overline{Z}_a - \overline{I}_g\, \overline{Z}\} \tag{10}$$

$$\Im\{\overline{V}_l\} = \Im\{\overline{V}_g + \overline{I}_l\, \overline{Z}_a - \overline{I}_g\, \overline{Z}\} \tag{11}$$

$$\Re\{\overline{I}_g\} = \Re\{\overline{I}_u - \overline{I}_l\} \tag{12}$$

$$\Im\{\overline{I}_g\} = \Im\{\overline{I}_u - \overline{I}_l\} \tag{13}$$

where the capital letters plus an over-line symbol designates the AC component of the variables. Note that the DC components are designated only with capital letters (no over-line).

2) DC component: The following expression is got from (1), (2) and (4):

$$I_l = I_u \tag{14}$$

$$V_{(h)_{DC}} = V_{(h)} - I_{(h)}\, R_a \tag{15}$$

B. Power balance

The net power balance across an arm has to be zero to keep the arm energy stable. This implies that the real AC power exchanged by the arm has to be equal to its DC power:

$$\Re\{\overline{V}_{(h)}\, \overline{I}^*_{(h)}\} + V_{(h)}\, I_{(h)} = 0 \tag{16}$$

C. Operating Setpoint Reference

Different control strategies could be considered depending on the operating requirements of the converter, e.g. P-Q or V_{DC}-Q control strategies [31]. Here, the P-Q control approach is considered such that a target AC grid current reference is calculated from the power setpoint. In addition, the reactive current of the grid is chosen to be equally shared between both arms. However, this particular condition could be different depending on the operating requirements.

$$\Im\{\overline{I}_u\} = \frac{\Im\{\overline{I}_g\}}{2} \tag{17}$$

D. Time-Domain Trajectories in Steady-State

The time domain trajectories of the arm currents and the modulated voltages are obtained by solving (8)-(17).

$$i_{(h)}(t) = I_{(h)} + |\overline{I}_{(h)}|\cos\left(2\omega t + \angle\overline{I}_{(h)}\right) \tag{18}$$

$$v_{(h)}(t) = V_{(h)} + |\overline{V}_{(h)}|\cos\left(2\omega t + \angle\overline{V}_{(h)}\right) \tag{19}$$

Next, the trajectory of the arm equivalent capacitor can be calculated considering their energy [33], [34]. The time-domain trajectories of the energy of each arm are obtained integrating their power over time:

$$\begin{aligned} e_{(h)}(t) &= \int i_{(h)}(t) \times v_{(h)}(t)dt \\ &= \frac{1}{2\omega}\Bigg(|\overline{I}_{(h)}||\overline{V}_{(h)}|\sin\left(2\omega t + \angle\overline{i}_{(h)} + \angle\overline{V}_{(h)}\right) \\ &+ 2\sqrt{2}\,V_{(h)}|\overline{I}_{(h)}|\sin\left(\omega t + \angle\overline{I}_{(h)}\right) \\ &+ 2\sqrt{2}\,I_{(h)}|\overline{V}_{(h)}|\sin\left(\omega t + \angle\overline{V}_{(h)}\right) \\ &+ 2\omega t\left(I_{(h)}V_{(h)} + |\overline{I}_{(h)}||\overline{V}_{(h)}|\cos\left(\angle\overline{I}_{(h)} - \angle\overline{V}_{(h)}\right)\right) \\ &+ e_{(h)_0}\Bigg) \end{aligned} \tag{20}$$

where $e_{(h)_0}$ is the initial energy of the arm.

Finally, the time domain voltage expression of the equivalent arm capacitor can be obtained from (20). Note that the arm equivalent capacitor voltage is approximately the sum of the voltages of the different SMs of the stack [29].

$$v_{c(h)}(t) = \sqrt{\frac{2\,e_{(h)}(t)}{C_a}} \tag{21}$$

IV. Controller Description

The MPC controller is designed to optimize the slow dynamics of the system and, consequently, its prediction horizon should be designed to be relatively long. Nevertheless, a direct implementation of the MPC with a long horizon and a fast sampling frequency could result in an optimal control problem with a large computational burden. This issue was discussed in [27], where a reduced sampling of the predictive algorithm combined with a cascaded structure was suggested. Indeed, the energy dynamics of the converter allow an MPC block with a reduced sampling to be considered. Nonetheless, because of the fast dynamics of the current, it could happen that the converter becomes unstable during sampling intervals. Thus, a fast inner controller is added to guarantee the good performance of the system even in the event of unexpected disturbances. On the other hand, a low sampling of the predictive regulator would also provide distorted signals to the inner control blocks. Consequently, the output of the predictive block is interpolated with the data of the prediction horizon such that smooth reference signals are obtained [27]. Then, the control system, apart from the MPC and the interpolation blocks, is formed by a Phase-Lock Loop (PLL) [35] used to determine the AC grid voltage and frequency, and a fast inner current controller tuned using an H_∞ approach [36]. Additionally, a Nearest Level Control (NLC) strategy is adopted to generate the firing signals and provide inter-arm energy balancing [37]. Note that the predictive algorithm is formulated to optimize the average dynamics of the system but it is not responsible of controlling the SMs individually. This last task is performed by the NLC algorithm, although other modulation techniques could be considered. The resulting control structure is shown in Fig. 2. The Operator Splitting Quadratic Program (OSQP) algorithm based on an Alternating Direction Method of Multipliers (ADMM) first-order method [38] is used to solve the optimal control problem of the predictive algorithm.

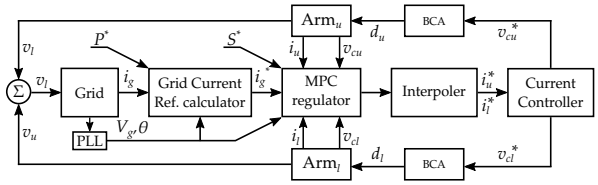

Fig. 2. Control schematic of the controller.

A. Linear Time-Varying Approximation

Even though the voltage-current circuit relationships of the system are linear, the power balance equations that relate arm currents and voltages with the arms energy are nonlinear. As it was discussed in [27], the addition of nonlinear terms on the formulation of the MPC algorithm largely increases the computational burden of the optimization. The use of an LTV-MPC approach is found convenient, because this approach provides an accurate approximation of the non-linear dynamics at a reduced computational cost [27]. Doing so, the nonlinear terms of the system are described as deviations around a steady-state trajectory varying periodically over time. Then, the nonlinear dynamics of the plant are approximated by linear ones and faster optimisation solvers can be used. The validity of this approximation is proven in Section VI where the LTV model is used to control a switching model of the MMC. In order to introduce the LTV approximation, x refers to a vector containing all the system states ($x \triangleq [i_{u_{[1]}}, i_{l_{[1]}}, v_{cu_{[1]}}, v_{cl_{[1]}}, \ldots, i_{u_{[N]}}, i_{l_{[}N], v_{cu_{[N]}}, v_{cl_{[N]}}}]^\intercal$) and u is a vector containing the control variables ($u \triangleq [v_{u_{[0]}}, v_{l_{[0]}}, \ldots, v_{u_{[N-1]}}, v_{l_{[N-1]}}]^\intercal$). Then, according to the previous description, the following definitions are done:

$$x = \widetilde{x} + \delta x \tag{22}$$

$$u = \widetilde{u} + \delta u \tag{23}$$

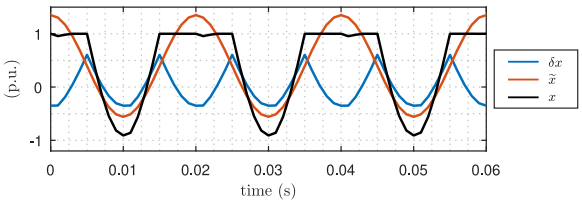

Fig. 3. Illustration of the LTV approximation.

where the accent $\sim$ designates steady-state periodic trajectories and δ designates variables that model disturbances around them. This approach is illustrated in Fig. 3. Besides, the system under analysis is assumed to be generically represented by:

$$\frac{d}{dt}x = f(x,u) \tag{24}$$

and trajectories of the system states can be linearised around a steady-state trajectory by applying a first-order Taylor's approximation as:

$$\begin{aligned}\frac{d}{dt}x &= \frac{d}{dt}(\widetilde{x}+\delta x) = \frac{d}{dt}\widetilde{x} + \frac{d}{dt}\delta x = f(x,u)\\ &\approx f(\widetilde{x},\widetilde{u}) + \left.\frac{\partial f}{\partial x}\right|_{\widetilde{x},\widetilde{u}}(x-\widetilde{x}) + \left.\frac{\partial f}{\partial u}\right|_{\widetilde{x},\widetilde{u}}(u-\widetilde{u})\\ &= \underbrace{f(\widetilde{x},\widetilde{u})}_{A_0} + \frac{f(\widetilde{x},\widetilde{u})}{\partial x}\delta x + \frac{f(\widetilde{x},\widetilde{u})}{\partial u}\delta u\end{aligned} \tag{25}$$

where the term A_0 corresponds to the steady-state trajectories at a particular time instant and it can be obtained from expressions (18)-(19) and (21).

B. LTV-MPC Algorithm

The LTV-MPC controller is formulated to track the current to be exchanged with the AC system, which is adapted according to the required power to be exchanged and the instantaneous grid voltage. This requirement is formulated as a constraint in order to guarantee that the current injection exactly follows the reference. According to their nature, the different parts of the optimization problems are described below.

1) Objective Function: its different terms account for the minimization of the arms current (i_u and i_l), the control voltages (v_u and v_l) and the reduction of the oscillation of the equivalent arm capacitor voltage (v_{cu} and v_{cl}), which is expected to be stabilized around the energy reference E_N (see Table I). The objective function is as following:

$$\begin{aligned}\min \quad & \sum_{k=1}^{N}\frac{\mathcal{S}}{\psi_1}(\delta v_{cu_{[k]}} + v_{ecu_{[k]}})^2 + \sum_{k=1}^{N}\frac{\mathcal{S}}{\psi_1}(\delta v_{cl_{[k]}} + v_{ecl_{[k]}})^2\\ &+ \sum_{k=1}^{N}\frac{\mathcal{R}}{\psi_2}(\delta i_{u_{[k]}} + i_{eu_{[k]}})^2 + \sum_{k=1}^{N}\frac{\mathcal{R}}{\psi_2}(\delta i_{l_{[k]}} + i_{el_{[k]}})^2\\ &+ \sum_{k=0}^{N-1}\frac{\mathcal{U}}{\psi_1}(\delta v_{u_{[k]}} + v_{eu_{[k]}})^2 + \sum_{k=0}^{N-1}\frac{\mathcal{U}}{\psi_1}(\delta v_{l_{[k]}} + v_{el_{[k]}})^2\end{aligned}$$

where $[k]$ describes a discrete time instant and N is the number of points of the perdiction horizon. Then, $\mathcal{R}$, $\mathcal{S}$ and $\mathcal{U}$ are weights and $\psi_{1,}$, ψ_2, ψ_3 are scaling factors. Note that i_{eu}, i_{el}, v_{ecu}, v_{ecl}, v_{eu} and v_{el} are variables that represent the difference between the steady-state trajectories and their references, e.g. $v_{ecu} = \widetilde{v}_{cu} - v^*_{cu}$.

2) Constraints: different types of constraints are introduced below according to their function.

a) Modelling: this set of constraints define the model of the predictive algorithm and correspond to the derivative terms of the LTV approximation (see Section IV-A). The discrete approximation of these terms is obtained applying a Forward Euler transformation:

$$\delta i_{(h)_{[k+1]}} = (1-\Delta t\frac{R_a}{L_a})\delta i_{(h)_{[k]}} - \frac{\Delta t}{L_a}\delta v_{(h)_{[k]}} \quad k=0,\dots,N-1 \tag{26}$$

$$\begin{aligned}\delta v_{c(h)_{[k+1]}} &= (1-\frac{\Delta t}{C_a}\frac{\widetilde{i}_{(h)_{[k]}}\widetilde{v}_{(h)_{[k]}}}{\widetilde{v}_{c(h)_{[k]}}})\delta v_{c(h)_{[k]}}\\ &+\frac{\Delta t}{C_a}\frac{\widetilde{v}_{(h)_{[k]}}}{\widetilde{i}_{(h)_{[k]}}}\delta i_{(h)_{[k]}} + \frac{\Delta t}{C_a}\frac{\widetilde{i}_{(h)_{[k]}}}{\widetilde{i}_{(h)_{[k]}}}\delta v_{(h)_{[k]}} \qquad k=0,\dots,N-1\end{aligned} \tag{27}$$

where Δt is the sampling interval. Note that (26) accounts for deviations around the steady-state trajectory of the arms current whereas (27) describes variations of the equivalent arms capacitor voltage.

b) Reference Tracking: considering (4), this equality constraint imposes that the current injected into the grid matches its reference.

$$\delta i_{u_{[k]}} - \delta i_{l_{[k]}} = \widetilde{i}_{l_{[k]}} - \widetilde{i}_{u_{[k]}} + i_{g_{[k]}} \quad k=1,\dots,N \tag{28}$$

c) System Limitations: the physical limits of the system are stated as inequality constraints that bound the upper and lower values of the variables. The following boundaries are considered:

$$0 \le \delta v_{(h)_{[k]}} + \widetilde{v}_{(h)} \quad k=0,\dots,N\text{-}1 \tag{29}$$

$$\delta v_{(h)_{[k]}} + \widetilde{v}_{(h)_{[k]}} + (\mathcal{V}-\lambda_{\mathcal{V}}) \le \widetilde{v}_{c(h)_{[k]}} + \delta v_{c(h)_{[k]}} \quad k=0,\dots,N\text{-}1 \tag{30}$$

$$-\lambda_i + \overset{\vee}{i} \le \widetilde{i}_{(h)_{[k]}} + \delta i_{(h)_{[k]}} \le \hat{i} + \lambda_i \quad k=1,\dots,N \tag{31}$$

$$\widetilde{v}_{c(h)_{[k]}} + \delta v_{c(h)_{[k]}} \le \hat{v}_c + \lambda_{v_c} \quad k=1,\dots,N\text{-}1 \tag{32}$$

$$0 \le \widetilde{v}_{c(h)_{[k]}} + \delta v_{c(h)_{[k]}} \le \hat{v}_c + \lambda_{v_c} \quad k=N \tag{33}$$

$$0 \le \lambda_i \le \overset{\wedge}{\lambda}_i \tag{34}$$

$$0 \le \lambda_{\mathcal{V}} \le \overset{\wedge}{\lambda}_{\mathcal{V}} \tag{35}$$

$$0 \le \lambda_{v_c} \le \overset{\wedge}{\lambda}_{v_c} \tag{36}$$

where $\vee$ and $\wedge$ denote lower and upper variable bounds respectively, $\mathcal{V}$ is a safety boundary and λ_i, $\lambda_{\mathcal{V}}$ and λ_{v_c} are slack variables introduced to soften the constraints (see Section VI for more detail about the use of the softening variables). Then, (29) and (30) limit the values of the modulated voltages ensuring that these signals are not negative and that they do not generate over-modulation by exceeding the arm capacitor voltage. Likewise, (31) limits the maximum value of the current through the arms. Next, (32) and (33) restrict the

TABLE I
CONVERTER/TUNING PARAMETERS.

Converter	Value	pu	Tuning	Value
V_g	335 kV	1	Δt	1 ms
V_{DC}	$\pm$ 525 kV	-	N	20 (0.02 s)
S_N	525 MW	1	$\psi_{1,2,3}$	1
E_N	8.87 MJ	-	$\mathcal{R}$	0.6
V_{DC}/V_{g_p}	1.10	1.10	$\mathcal{S}$	0.4
N_{arm}	589	-	$\mathcal{U}$	10^{-3}
C_{SM}	9.2 mF	34 kJ/MVA	W_{λ_i}	50
L_a	102.1 mH	15 %	$W_{\lambda_v,\lambda_{vc}}$	10
L	68 mF	10 %	$\overset{\vee}{v_c}$, $\overset{\wedge}{v_c}$	0 MV, 1.18 MV
R_a	0.85 Ω	0.4 %	$\hat{i}$, $\overset{\vee}{i}$	-1.78 kA, 1.78 kA
R	0.85 Ω	0.4 %	$\mathcal{V}^*$	3%
I_p	1.78 kA	1.136	$\overset{\wedge}{\lambda}{}^*_i$	10%
V_{SM}	1.81 kV	0.0054	$\overset{\wedge}{\lambda}{}^*_{v_c}$	3%
V_{SM_p}	2.01 kV	0.06	$\overset{\wedge}{\lambda}{}^*_v$	3%

* The percentage refers to the base value of this parameter.

maximum voltage of the equivalent arm capacitor over the prediction horizon. Finally, (34)-(36) bound the values of the softening variables, if required.

C. LTV-MPC Tuning Parameters

The LTV-MPC algorithm described in this document is equivalent to the controller presented in [27]. The algorithm is defined in per-unit values and the tuning is based on the fact that the system states present a negative correlation, i.e. a reduction on the equivalent capacitor voltage requires the injection of circulating current, which increases the current through the arms. Because of this negative correlation, the weights of these terms are defined as: $\mathcal{S} + \mathcal{R} = 1$. It is desired that the control action has a negligible impact on the steady-state performance; thus, a very low weight is assigned to this parameter ($\mathcal{U} \sim 10^{-3}$). In addition, the scaling factors ψ_1, ψ_2 and ψ_3 are included in the formulation to normalize the objective function. However, as per-unit values are used to formulate the algorithm, these terms are set equal to 1 (see Table I). The effect of considering different weights under nominal operating conditions is depicted in Fig. 4. It is shown that different weights cause a different injection of circulating current through the converter, which also affects the voltage ripple oscillation of the arm in steady-state. On the other hand, it is found that the performance of the converter when its nominal operating ratings are exceeded differs from the analysis presented in [27], as a result of numerous system states reaching their physical limits. Note that these limits cannot be exceeded because of the hard constraints defined in the predictive algorithm. Under these circumstances, it is observed that the weighting factor is mostly relevant for the transient response of the converter but do not significantly change the operating area in steady-state. Additionally, it must be mentioned that the algorithm can be tuned to present a conventional performance under nominal operating conditions such that the injection of harmonic components into the circulating current is only performed when the system is driven beyond its nominal ratings. Doing so, it can be argued that the system efficiency is not affected during nominal operating

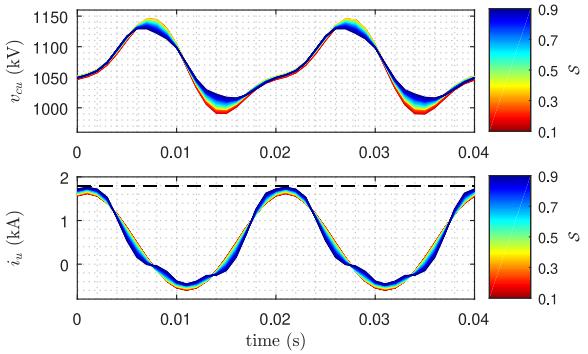

Fig. 4. Upper arm trajectories at different $\mathcal{S}$ weights.

conditions. Therefore, only one weighting factor is considered in the subsequent study.

The sampling frequency and the horizon length are chosen considering their impact on the performance and the computational burden. The sampling frequency is chosen relatively low considering the slow energy dynamics of the SMs and the prediction horizon is chosen sufficiently large to adequately foresee the impact of the control action. Fig. 5 shows the influence of these parameters on the states trajectories. The tuning values of the algorithm are detailed in Table I.

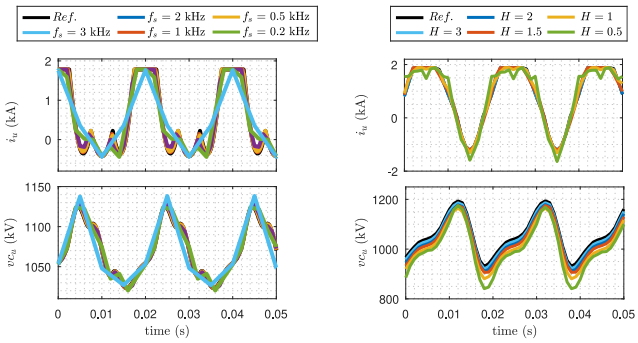

(a) Sampling frequency. (b) Prediction horizon length.

Fig. 5. Effect of the sampling frequency and prediction horizon on the system's states. Note that H refers to the number of fundamental periods of the predictive horizon.

The dynamic behaviour of the the system is depicted in in Fig. 6. This simulation starts at zero load and later, at time 0.01 s, the power reference is modified and a step-change from

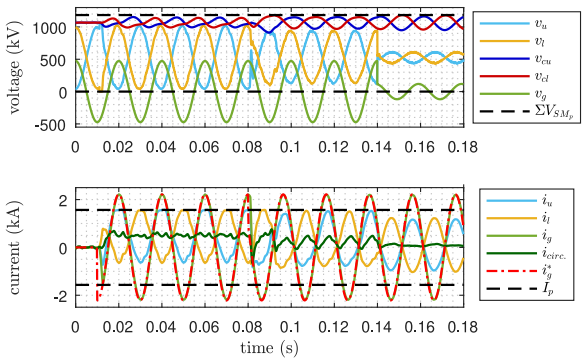

Fig. 6. Dynamic performance of the LTV-MPC algorithm ($\mathcal{S}$ = 0.4).

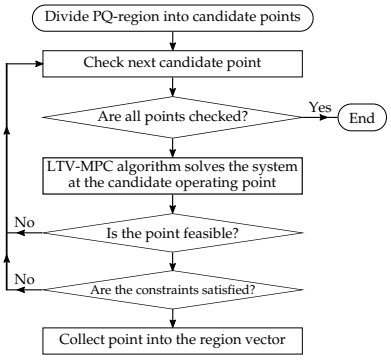

Fig. 7. Flowchart of the sequential search algorithm.

0 to 1 pu (power factor equal to 1) is performed. Next, at time 0.08 s, the power reference undergoes another step-change and the power factor changes from 1 to 0.4. Finally, at time 0.14 s, the AC grid undergoes a fault and its voltage falls to 20 % of its nominal value and the phase shifts by 15°. It is seen that the cascaded controller keeps the system stable at all times and exhibits good transient response. This graph proves the good performance of the controller under nominal operating conditions before analysing the response of the system when the power ratings of the converter are exceeded.

V. Operating Region Analysis

The underlying numerical optimization of the predictive algorithm does not permit a closed solution of the system trajectories to be obtained. Thus, the operating area of the converter is analyzed using a numerical method based on a sequential search algorithm. The search strategy is used to evaluate the feasible operating region of the system under two scenarios: when the converter is driven by a conventional controller and when the MPC controller is used. Note that a conventional controller is considered to be a control structure based on cascaded PI loops and sinusoidal current references as described in [31]. In order to determine the ideal operating region, it is assumed that the output trajectories of the controllers match the ones followed by the plant. Nevertheless, detailed simulations considering the effect of the different control blocks described in Section IV are presented in Section VI to validate the performance of the controller.

A. Sequential Search Algorithm

The capability curve of the converter is evaluated by sampling the potential P-Q region of the device. These samples must be small enough to be representative of the area of operation. Each of these samples represents a grid current reference point at which the converter should be operated. Then, the system is driven from no load to the reference point. The search of suitable points is done radially, i.e., the region under analysis is divided into small angle increments and for each of these angles the radius is swept from 0 to 2 pu. The sequential search algorithm evaluates whether or not the system could be driven to that specific reference point. Once a candidate point has been assessed, the next point is evaluated. The flowchart of the search strategy is shown in Fig 7.

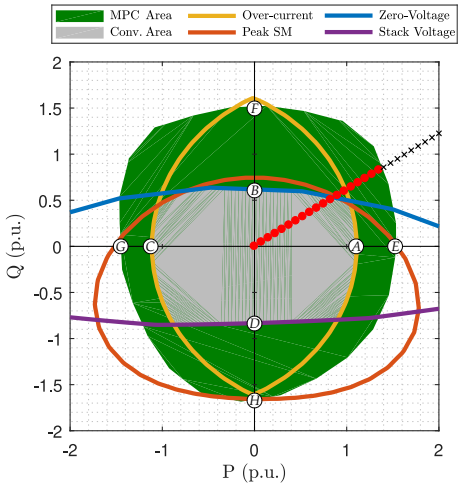

Fig. 8. Comparison of the operating region. The radial search is exemplified with symbols ● and ×, which denote feasible and unfeasible points. In order to provided more insight about the behaviour of the predictive algorithm, different points marked in this picture are further analyzed in Fig. 9 and Fig. 10.

B. P-Q Region

The results obtained from the sequential search are presented in Fig. 8. The operating area of the converter considering a conventional control strategy is depicted in gray. This area is limited by the following boundaries [39]:

- Over-current: current that each arm can withstand.
- Peak SM: voltage that a stack of SMs could withstand.
- Zero-Voltage: capability to generate negative voltage. As half-bridge SMs are considered, it is not possible to generate negative voltage.
- Stack Voltage: voltage that a stack of SMs can synthesize considering their available energy.

Similarly, the area obtained using the LTV-MPC approach is shown green. These areas correspond to the converter parameters shown in Table I.

Next, Fig. 9 shows the trajectories of the system variables when the converter is driven by conventional control references. Note that the operating area of the converter is not symmetrical and it depends on which constraints are met at different directions. Then, points *A* and *C* are found when the upper or lower current limits are reached. Likewise, boundary *B* is formed as a results of the in-ability to generate negative voltage. Finally, point *D* is obtained when there is not enough energy stored in the SMs of the arms to modulate the required voltage.

Fig. 10 shows how the trajectories of points *E*, *F*, *G* and *H* are regulated by the LTV-MPC algorithm such that the system variables do not reach their limits at points *A*, *B*, *C* and *D*. This, however, is subject to the thermal limitations of the converter which are not considered here. The analysis of the trajectories in Fig. 10 brings significant findings. First, the increment of the operating region is not homogeneous in all directions and it is noticeable that different strategies are inherently adopted by the MPC algorithm. The comparison between points *A* (Fig. 9) and *E* (Fig. 10) indicate the injection of circulating current. This is noticeable from the harmonic analysis depicted

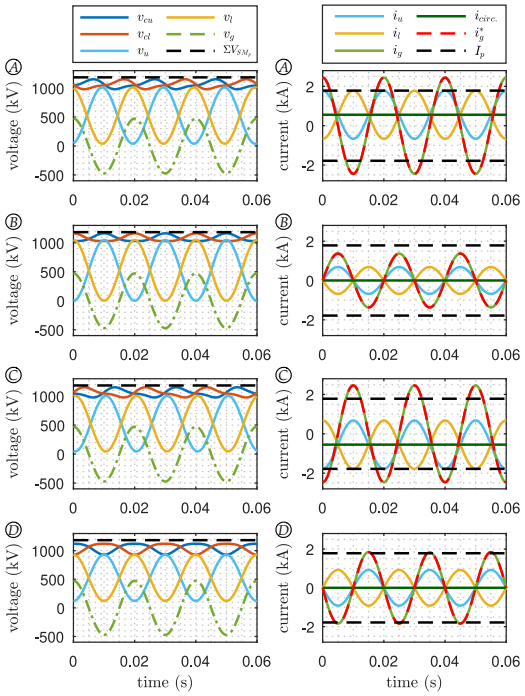

Fig. 9. Trajectories of points *A, B, C* and *D* marked in Fig. 8.

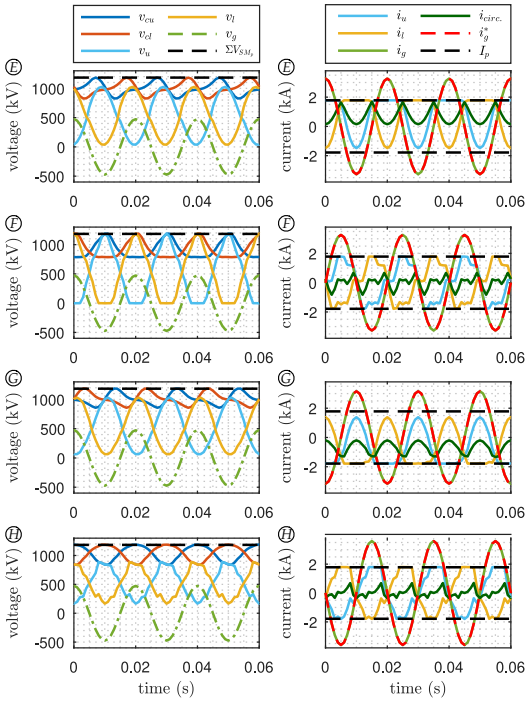

Fig. 10. Trajectories of points *E, F, G* and *H* marked in Fig. 8

in Fig. 11, which shows that the injection of current through the arms is not limited to a single component but varies depending on the operating conditions. Likewise, it is evident from comparing points *B* and *F* that the MPC algorithm modified the average energy stored in the SMs. The later, combined with an appropriate injection of circulating current, permitted to extend the operating area. Thus, it is observed that the predictive controller enhances the operating area of the

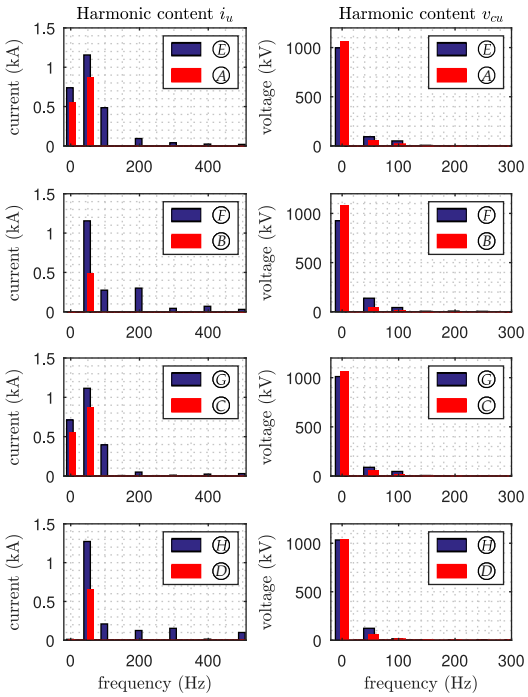

Fig. 11. Harmonic analysis of trajectories i_u and v_{cu} at points depicted in Fig. 8.

converter by naturally combining different strategies present in the literature [12], [13], [15]. Furthermore, the trajectories of the system variables are adapted online which implies that the change of the system trajectories is done by considering the values of the states at each moment and they are adapted for each operating condition.

C. Operating region under different design parameters

In order to evaluate the influence of the design parameters on the operating region, Fig. 12 shows the P-Q area of the converter when these parameters are slightly modified. Based on this information, three study cases are considered (see Table II). Fig. 13 compares the feasible region of the converter using the MPC strategy and the conventional controller for the three different study cases. The results are summarized in Table III, which provides information about the increment of apparent power the converter could exchange in each scenario. Nevertheless, it is not possible to generally quantify this increment as the operating area is not enhanced evenly for all power angles. Thus, only specific directions are compared in Table III. Finally, the results indicate that despite the variation on the converter parameters, the MPC strategy significantly increase the operating area of the converter, which in the worst case and direction is enhanced by up to 25 %.

VI. Simulation Results

This section presents detailed simulation results to validate the performance of the LTV-MPC strategy at points *E* and *H*. These simulations, conducted in Matlab Simulink, are based on a switching model of the converter where each arm is built

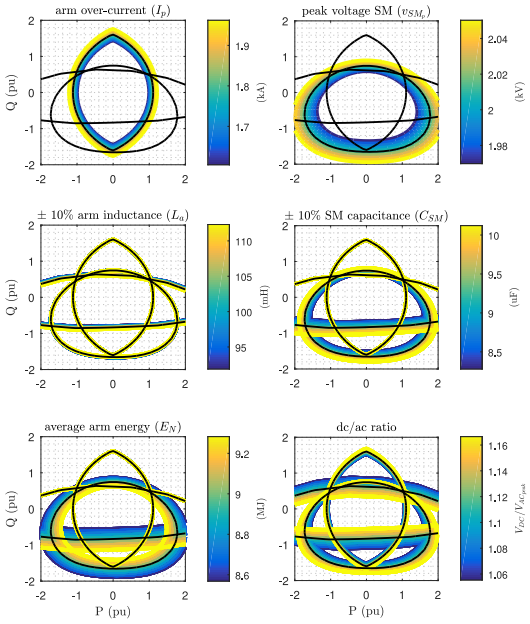

Fig. 12. Sensitivity analysis of the operating region. As a reference, the base region of the converter (see in Table I) is plot in black.

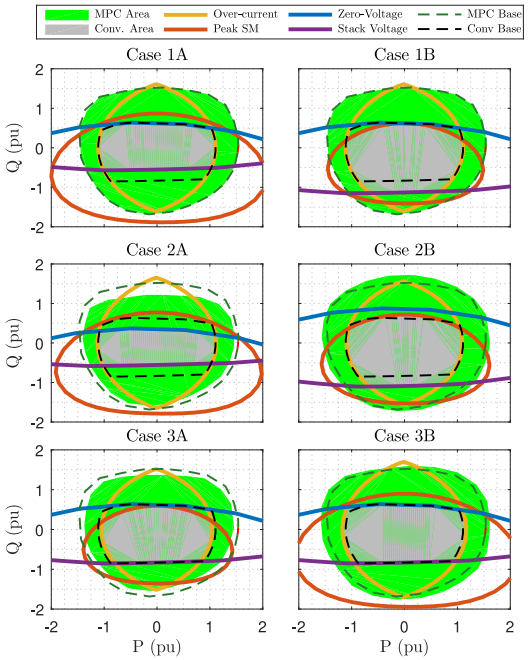

Fig. 13. Feasible region: MPC vs conventional control. The base regions are plot in dashed lines.

by a stack of 589 SMs. The output voltage is synthesized by implementing a NLC strategy [8]. As the system is driven to operate at its operating boundaries, it is expected that a small deviation from the ideal model used in Section V-B might make the optimal control problem become unfeasible. This is justified as the ideal trajectories presented in Section V might slightly mismatch with the detailed dynamics of the system. Thus, softening slack variables are considered in order to allow small violations of the rated constraints, if required. Besides, the soft constraints are also bounded to not produce

TABLE II
PARAMETERS OF THE SENSBILITY STUDY CASES.

		I_p (kA)	V_{SM_p} (kV)	E_{SM} (kJ)	V_g
Case 1	A	1.78	2.01	14.77 (-2%)	335
	B	1.78	2.01	15.37 (+2%)	335
Case 2	A	1.78	2.01	15.07	352 (+5%)
	B	1.78	2.01	15.07	318 (-5%)
Case 3	A	1.6 (-10%)	1.81 (-10%)	15.07	335
	B	1.96 (+10%)	2.21 (+10%)	15.07	335

TABLE III
INCREMENT OF OUTPUT APPARENT POWER AT SPECIFIC ANGLES.

	Case 1		Case 2		Case 3	
Power angle (ϕ)	A	B	A	B	A	B
0	40%	45%	27%	47%	37%	46%
$\pi/2$	85%	85%	78%	95%	74%	89%
π	30%	30%	25%	40%	26%	35%
$-\pi/2$	105%	46%	91%	50%	64%	85%

a large transgression of the physical constraints. These slack variables are added into the objective function and are heavily penalized with weights $\mathcal{W}_{\lambda_i}$, $\mathcal{W}_{\lambda_v}$ and $\mathcal{W}_{\lambda_{vc}}$ respectively. The tuning and the simulation parameter values are presented in Table I.

First, Fig. 14 shows the performance of the system at point *E*. The simulation begins at 1 pu (power factor 1) and at time 0.03 s the reference is smoothly changed to reach 1.48 pu (power factor 1) at time 0.05 s. It is noticeable how the LTV-MPC algorithm modifies the natural trajectories of the plant such that this point is achievable. Nevertheless, as it was expected, the non-ideal elements of the model cases the trajectories predicted by the predictive algorithm to slightly deviate from the dynamics of the ideal system shown in Fig. 10. In order to relax the optimization constraints, the slack variables acquire non-zero values. This is shown in Fig. 14 where the values of the softening variables are plotted. Note that before exceeding 1 pu the MPC algorithm controls the system without requiring the use of additional allowance. Nevertheless, the margins provided to the softening variables are considered reasonable for a realistic operation of the converter. In addition, the voltage of a few SMs is also displayed, proving the good balancing of the SMs and the compatibility between the balancing strategy and the predictive algorithm. Likewise, Fig. 15 shows the performance of the system at point *H*. Here, the system is driven from 1 pu (power factor 0) to 1.475 pu (power factor 0) between the time instants 0.03 s and 0.05 s. Similarly, the trajectories resemble the ones shown in Fig. 10 although the soft-constraints acquire non-zero values at specific instants of time such that the problem does not become infeasible.

VII. CONCLUSION

This paper has proposed a control structure based on an MPC strategy to investigate how the operating region of an MMC could be extended. It has been shown that when compared with a conventional controller with classical sinusoidal current references, the predictive strategy can naturally extend

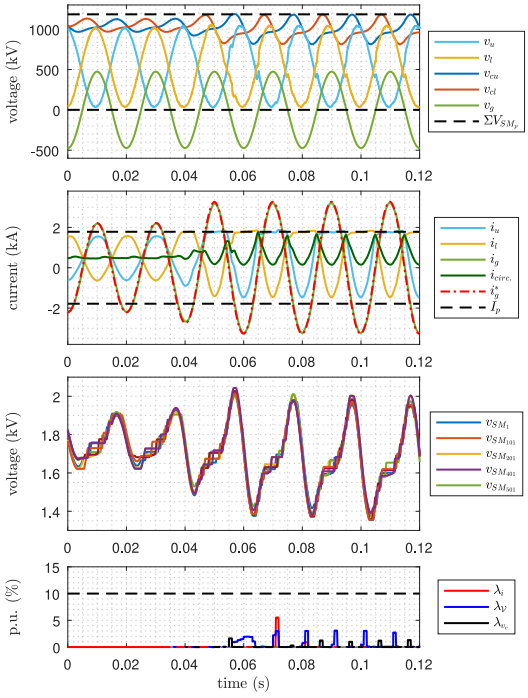

Fig. 14. Simulation results at operating point *E*.

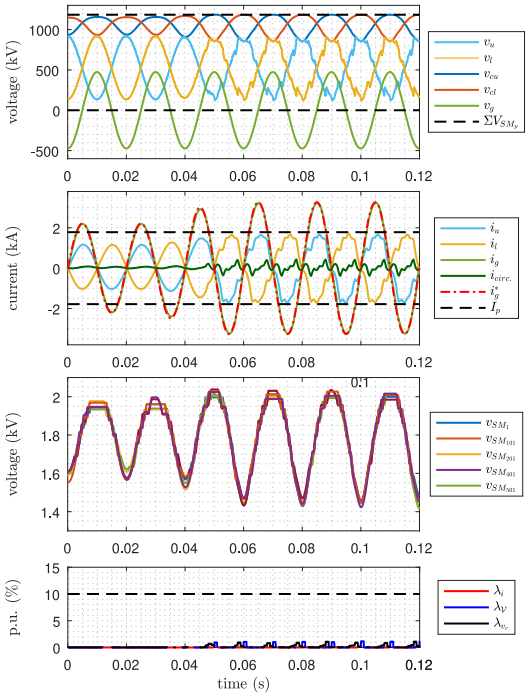

Fig. 15. Simulation results at operating point *H*.

the P-Q area of the MMC by adjusting the trajectories of the system variables. To achieve this, the predictive controller naturally combines different strategies, such as the circulating current injection and the regulation of the average energy of the SMs. Thereby, the feasible operating limits of the converter show that the converter can be steadily operated above its nominal design ratings allowing a better utilization of the hardware resources.

REFERENCES

[1] H. Akagi, "Classification, terminology, and application of the modular multilevel cascade converter (mmcc)," *IEEE Trans. Power Electron.*, vol. 26, no. 11, pp. 3119–3130, Nov 2011.

[2] M. Saeedifard and R. Iravani, "Dynamic performance of a modular multilevel back-to-back hvdc system," *IEEE Trans. Del.*, vol. 25, no. 4, pp. 2903–2912, Oct 2010.

[3] G. T. Son, H. Lee, T. S. Nam, Y. Chung, U. Lee, S. Baek, K. Hur, and J. Park, "Design and control of a modular multilevel hvdc converter with redundant power modules for noninterruptible energy transfer," *IEEE Trans. Del.*, vol. 27, no. 3, pp. 1611–1619, July 2012.

[4] T. H. Nguyen, K. A. Hosani, M. S. ElMoursi, and F. Blaabjerg, "An overview of modular multilevel converters in hvdc transmission systems with statcom operation during pole-to-pole dc short circuits," *IEEE Trans. Power Electron.*, pp. 1–1, 2018.

[5] A. Lesnicar and R. Marquardt, "An innovative modular multilevel converter topology suitable for a wide power range," in *2003 IEEE Bologna Power Tech Conf. Proc.,*, vol. 3, June 2003, pp. 6 pp. Vol.3–.

[6] Q. Yang, J. Qin, and M. Saeedifard, "Analysis, detection, and location of open-switch submodule failures in a modular multilevel converter," *IEEE Trans. Del.*, vol. 31, no. 1, pp. 155–164, Feb 2016.

[7] C. Oates, "Modular multilevel converter design for vsc hvdc applications," *IEEE J. Emerg. Sel. Topics Power Electron.*, vol. 3, no. 2, pp. 505–515, June 2015.

[8] Q. Tu, Z. Xu, and L. Xu, "Reduced switching-frequency modulation and circulating current suppression for modular multilevel converters," *IEEE Trans. Del.*, vol. 26, no. 3, pp. 2009–2017, July 2011.

[9] M. Vasiladiotis, N. Cherix, and A. Rufer, "Accurate capacitor voltage ripple estimation and current control considerations for grid-connected modular multilevel converters," *IEEE Trans. Power Electron.*, vol. 29, no. 9, pp. 4568–4579, Sept 2014.

[10] R. Picas, J. Pou, S. Ceballos, V. G. Agelidis, and M. Saeedifard, "Minimization of the capacitor voltage fluctuations of a modular multilevel converter by circulating current control," in *IECON 2012 - 38th Annu. Conf. on IEEE Ind. Electron. Soc.*, Oct 2012, pp. 4985–4991.

[11] J. Pou, S. Ceballos, G. Konstantinou, V. G. Agelidis, R. Picas, and J. Zaragoza, "Circulating current injection methods based on instantaneous information for the modular multilevel converter," *IEEE Trans. on Ind. Electron.*, vol. 62, no. 2, pp. 777–788, Feb 2015.

[12] H. Kim, S. Kim, Y. H. Chung, D. W. Yoo, C. K. Kim, and K. Hur, "Operating region of modular multilevel converter for hvdc with controlled second-order harmonic circulating current: Elaborating p-q capability," *IEEE Trans. Del.*, vol. 31, no. 2, pp. 493–502, April 2016.

[13] K. Ilves, A. Antonopoulos, L. Harnefors, S. Norrga, L. Ängquist, and H. P. Nee, "Capacitor voltage ripple shaping in modular multilevel converters allowing for operating region extension," in *IECON 2011 - 37th Annu. Conf. of the IEEE Ind. Electron. Soc.*, Nov 2011, pp. 4403–4408.

[14] I. M. Sanz, P. D. Judge, C. E. Spallarossa, B. Chaudhuri, and T. C. Green, "Dynamic overload capability of vsc hvdc interconnections for frequency support," *IEEE Trans. Energy Convers.*, vol. 32, no. 4, pp. 1544–1553, Dec 2017.

[15] S. Norrga, L. Ängquist, and K. Ilves, "Operating region extension for multilevel converters in hvdc applications by optimisation methods," in *10th IET Int. Conf. on AC and DC Power Transmission (ACDC 2012)*, Dec 2012, pp. 1–6.

[16] S. Norrga, L. Ängquist, K. Ilves, L. Harnefors, and H. P. Nee, "Frequency-domain modeling of modular multilevel converters," in *IECON 2012 - 38th Annu. Conf. on IEEE Ind. Electron. Soc.*, Oct 2012, pp. 4967–4972.

[17] M. A. Perez, J. Rodriguez, E. J. Fuentes, and F. Kammerer, "Predictive control of ac-ac modular multilevel converters," *IEEE Trans. Ind. Electron.*, vol. 59, no. 7, pp. 2832–2839, July 2012.

[18] L. Ben-Brahim, A. Gastli, M. Trabelsi, K. A. Ghazi, M. Houchati, and H. Abu-Rub, "Modular multilevel converter circulating current reduction using model predictive control," *IEEE Trans. Ind. Electron.*, vol. 63, no. 6, pp. 3857–3866, June 2016.

[19] C. Bordons and C. Montero, "Basic Principles of MPC for Power Converters: Bridging the Gap Between Theory and Practice," *IEEE Ind. El ectron. Mag.*, vol. 9, no. 3, pp. 31–43, sep 2015.

[20] J. Moon, J. Gwon, J. Park, D. Kang, and J. Kim, "Model predictive control with a reduced number of considered states in a modular multilevel converter for hvdc system," *IEEE Trans. Del.*, vol. 30, no. 2, pp. 608–617, April 2015.

[21] B. S. Riar, T. Geyer, and U. K. Madawala, "Model predictive direct current control of modular multilevel converters: Modeling, analysis, and experimental evaluation," *IEEE Trans. Power Electron.*, vol. 30, no. 1, pp. 431–439, Jan 2015.

[22] K. Ilves, L. Harnefors, S. Norrga, and H. Nee, "Predictive sorting algorithm for modular multilevel converters minimizing the spread in the submodule capacitor voltages," *IEEE Trans. Power Electron.*, vol. 30, no. 1, pp. 440–449, Jan 2015.

[23] S. Vazquez, J. Rodriguez, M. Rivera, L. G. Franquelo, and M. Norambuena, "Model predictive control for power converters and drives: Advances and trends," *IEEE Trans. Ind. Electron.*, vol. 64, no. 2, pp. 935–947, Feb 2017.

[24] T. Geyer, *Model Predictive Control of High Power Converters and Industrial Drives*. Wiley, 2016.

[25] Z. Gong, X. Wu, P. Dai, and R. Zhu, "Modulated model predictive control for mmc-based active front-end rectifiers under unbalanced grid conditions," *IEEE Trans. Ind. Electron.*, vol. 66, no. 3, pp. 2398–2409, March 2019.

[26] D. Zhou, S. Yang, and Y. Tang, "Model-predictive current control of modular multilevel converters with phase-shifted pulsewidth modulation," *IEEE Trans. Ind. Electron.*, vol. 66, no. 6, pp. 4368–4378, June 2019.

[27] J. M. Rodriguez-Bernuz and A. Junyent-Ferré, "Model predictive circulating current regulator for single-phase modular multilevel converter," in *IEEE Energy Convers. Congr. Expo. (ECCE)*, Sept 2018, pp. 1–7.

[28] M. A. Perez, S. Bernet, J. Rodriguez, S. Kouro, and R. Lizana, "Circuit topologies, modeling, control schemes, and applications of modular multilevel converters," *IEEE Trans. Power Electron.*, vol. 30, no. 1, pp. 4–17, Jan 2015.

[29] L. Harnefors, A. Antonopoulos, S. Norrga, L. Ängquist, and H. P. Nee, "Dynamic analysis of modular multilevel converters," *IEEE Trans. Ind. Electron.*, vol. 60, no. 7, pp. 2526–2537, July 2013.

[30] U. N. Gnanarathna, A. M. Gole, and R. P. Jayasinghe, "Efficient modeling of modular multilevel hvdc converters (mmc) on electromagnetic transient simulation programs," *IEEE Trans. Del.*, vol. 26, no. 1, pp. 316–324, Jan 2011.

[31] E. Prieto-Araujo, A. Junyent-Ferré, C. Collados-Rodríguez, G. Clariana-Colet, and O. Gomis-Bellmunt, "Control design of modular multilevel converters in normal and ac fault conditions for hvdc grids," *Electric Power Systems Research*, vol. 152, pp. 424 – 437, 2017.

[32] M. Hagiwara and H. Akagi, "Control and experiment of pulsewidth-modulated modular multilevel converters," *IEEE Trans. Power Electron.*, vol. 24, no. 7, pp. 1737–1746, July 2009.

[33] K. Ilves, A. Antonopoulos, S. Norrga, and H. P. Nee, "Steady-state analysis of interaction between harmonic components of arm and line quantities of modular multilevel converters," *IEEE Trans. Power Electron.*, vol. 27, no. 1, pp. 57–68, Jan 2012.

[34] K. Ilves, S. Norrga, L. Harnefors, and H. P. Nee, "On energy storage requirements in modular multilevel converters," *IEEE Trans. Power Electron.*, vol. 29, no. 1, pp. 77–88, Jan 2014.

[35] S. Golestan, M. Monfared, F. D. Freijedo, and J. M. Guerrero, "Dynamics assessment of advanced single-phase pll structures," *IEEE Trans. Ind. Electron.*, vol. 60, no. 6, pp. 2167–2177, June 2013.

[36] S. Skogestad and I. Postlethwaite, *Multivariable Feedback Control: Analysis and Design*. Wiley, 2005.

[37] Q. Tu and Z. Xu, "Impact of sampling frequency on harmonic distortion for modular multilevel converter," *IEEE Trans. Power Del.*, vol. 26, no. 1, pp. 298–306, Jan 2011.

[38] B. Stellato, G. Banjac, P. Goulart, A. Bemporad, and S. Boyd, "OSQP: An operator splitting solver for quadratic programs," *ArXiv e-prints*, Nov. 2017.

[39] P. D. Judge, G. Chaffey, M. M. C. Merlin, P. R. Clemow, and T. C. Green, "Dimensioning and modulation index selection for the hybrid modular multilevel converter," *IEEE Trans. Power Electron.*, vol. 33, no. 5, pp. 3837–3851, May 2018.